Effect of Functionalized Gold Nanoparticles on Floating Lipid Bilayers

Sabina Tatur,*,† Marco Maccarini,*,‡,∥ Robert Barker,‡ Andrew Nelson,§ and Giovanna Fragneto‡

†Department of Physics, University of Illinois at Chicago, 845 West Taylor Street, Chicago, Illinois 60607, United States
‡Institut Laue-Langevin, 6 rue Jules Horowitz, 38042 Grenoble, France
§Australian Nuclear Science and Technology Organisation, Locked Bag 2001, Kirrawee DC NSW 2232, Australia

Ⓢ Supporting Information

ABSTRACT: The development of novel nano-engineered materials poses important questions regarding the impact of these new materials on living systems. Possible adverse effects must be assessed in order to prevent risks for health and the environment. On the other hand, a thorough understanding of their interaction with biological systems might also result in the creation of novel biomedical applications. We present a study on the interaction of model lipid membranes with gold nanoparticles (AuNP) of different surface modifications. Neutron reflectometry experiments on zwitterionic lipid double bilayers were performed in the presence of AuNP functionalized with cationic and anionic head groups. Structural information was obtained that provided insight into the fate of the AuNPs with regard to the integrity of the model cell membranes. The AuNPs functionalized with cationic head groups penetrate into the hydrophobic moiety of the lipid bilayers and cause membrane disruption at an increased concentration. In contrast, the AuNPs functionalized with anionic head groups do not enter but seem to impede the destruction of the lipid bilayer at an alkaline pH. The information obtained might influence the strategy for a better nanoparticle risk assessment based on a surface charge evaluation and contribute to nano-safety considerations during their design.
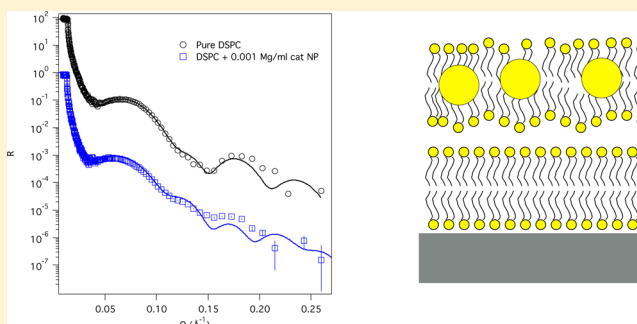
INTRODUCTION

In recent years, gold nanoparticles (AuNPs) have become more and more attractive for biomedical and pharmaceutical applications due to their unique optical, electronic, and thermal properties, as well as their straightforward synthesis, stability, and the simple incorporation of secondary tags for cell recognition.[1−6] The increasing variety of applications includes gene therapy, cancer therapy, targeted delivery of drugs and antigens, biosensors, and optical bioimaging.[1,2,7,8] The use of AuNPs is, however, a mixed blessing since it also involves potential risks of harmful side effects on health and the environment. A careful risk assessment is therefore needed to ensure safe clinical practice and handling before these nanotools become widely available.

A key issue in making use of AuNPs for biomedical purposes is an understanding of their interaction with cells beyond the designated functions. Since the first contact that all nanomaterials will always have with any living organism is through the cell membrane, a ∼5 nm thick lipid bilayer, this study focuses on the interaction of AuNPs with model cell membranes and will discuss the effect of surface charge on AuNP destiny and membrane integrity.

Previous research done in this field showed that AuNPs reveal cytotoxic effects dependent on their concentration, size, surface modification, and charge.[8−12] The formation of nanoscale holes was observed in model biomembranes, as well as in living cell membranes, where the degree of membrane disruption was dependent on the lipid bilayer phase state.[13−17] So far, only symptomatic experimental analysis in this field was performed and there is still a lack in the systematic approach to understand the correlation between the surface characteristics of cell membranes and AuNPs, in regard to a potential cell membrane damage that might lead to cell malfunction and death.

To provide insight into the fate of AuNPs and their impact on cell membrane integrity, the interaction of two classes of AuNPs with single component model membranes was analyzed. Two nanometer diameter AuNPs functionalized with cationic [N,N,N-trimethyl (11-mercaptoundecyl) ammonium] and anionic (mercaptoundecanoic acid) surface groups were brought into contact with single-component zwitterionic DSPC (1,2-distearoyl-sn-glycero-3-phosphocholine) double bilayers. The single component membranes served as simple models in order to focus on the issue of the interaction of AuNPs with two lipid phases (i.e., gel and fluid phase), without the complications arising from changes in structure and

organization of the lipid bilayer as a result of additional components in the membrane. Lipids with zwitterionic phosphocholine head groups are the most common components of the eukaryotic cell membrane and the ideal lipid substitute for simple model cell membranes.[18]

If a single lipid bilayer is directly adsorbed onto a solid substrate, they mutually exert a strong electrostatic interaction that might change the lipid phase behavior and influence stability studies of the model membrane.[20,21] A lipid double bilayer, in which a second bilayer floats at 20−30 Å on top of the first one, gives access to a highly hydrated, fluctuating bilayer that represents a membrane system with dynamic properties comparable to biological membranes and is greatly relevant for the examination of the influence of AuNPs on lipid membrane structure and integrity.[22]

There are several advantages of using the neutron reflectivity technique for this kind of study. Neutrons have a weak interaction with matter because they are not charged and perturb soft matter systems very little. Neutrons are therefore deeply penetrating, making them ideal probes for buried interfaces. Last, but not least, with the use of isotopic substitution, we can vary the contrast between different regions of the system, highlighting the scattering of each component of the system. This greatly aids structural determination.

Taken together, this study provides insight into the fate of functionalized AuNPs with regard to the integrity of model cell membranes. Futhermore, it will allow an initial risk assessment based on a surface charge evaluation and contribute to the future design of new particles with an improved hazard profile.

■ MATERIALS AND METHODS

Chemicals. DSPC (1,2-distearoyl-*sn*-glycero-3-phosphocholine) were obtained in powder form (chemical purity >99%) from Avanti Polar Lipids (Alabaster, AL; chemical purity >99%) and dissolved without further purification in spectrograde chloroform (Sigma-Aldrich) to prepare solutions of 1 mM total lipid concentration. Distilled water was purified with a Milli-Q Gradient System (Millipore, Bedford, MA) to produce ultrapure water with a resistivity of 18.2 MΩ cm. Octanethiol ($C_8H_{18}SH$, 99%), 11-mercaptoundecanoic acid [$HS(CH_2)_{10}CO_2H$, 98%], hydrogen tetrachloroaurate(III) trihydrate ($HAu^{III}Cl_4 \cdot 3H_2O$, ≥ 99.9%), sodium borohydride ($NaBH_4$, 99%), and tetraoctyl-ammonium bromide [$(C_8H_{17})_4NBr$, 98%] were obtained from Sigma-Aldrich and used as received for the gold nanoparticle preparation.

Nanoparticle Preparation. The gold nanoparticles were fabricated as described by McIntosh et al.[23] First, octanethiolate-capped gold nanoparticles (C_8SAu NPs) were synthesized following the two-phase method developed by Brust et al. as previously reported.[24,25] The C_8SAu NPs were analyzed by TEM (Philips CM200; 200 kV), UV−vis (Cary Bio-100, Varian Inc., Palo Alto, CA), and TGA (Thermal TGA 2950, TA Instruments, New Castle, DE) to determine their average diameter (2 ± 0.5 nm), their surface coverage (0.59 ± 0.03 ligands per surface gold atom), and their average molecular mass (52000 ± 8000 g mol^{-1}). The anion-functionalized and cation-functionalized AuNPs were then prepared via Murray place−displacement reaction of the 2 nm C_8SAu NPs.[26] For the preparation of the anionic carboxylic acid-functionalized AuNPs, 740 mg of 11-mercaptoundecanoic acid was added to 140 mg of C_8SAu NPs in 4 mL of tetrahydrofuran and stirred for two days under argon at room temperature. Mixed monolayer protected gold nanoparticles functionalized with ω-thiol carboxylic acid, and octanethiol ligands (COOHAu NPs) were generated and precipitated in the form of a black powder. The solvent was rotavaporated, and the remaining solid was exhaustively washed by repeated suspension, centrifugation, and decantation with dichloromethane.[27] The composition of the AuNPs was examined by ^{1}H NMR and indicated that ~50% of the original

octanethiol ligand was exchanged to the ω-thiol carboxylic acid. The COOHAu NPs solubilized in an aqueous solution of sodium hydroxide of pH 12. In a similar procedure, the cationic trimethylammonium-functionalized AuNPs were prepared by stirring 150 mg of C_8SAu NPs and 150 mg of N,N,N-trimethyl(11-mercaptoundecyl)ammonium chloride in 20 mL of degassed tetrahydrofuran under argon for two days at room temperature. The cationic thiol was synthesized according to a procedure reported by Tien et al.[28] The black precipitate of the gold nanoparticles protected by a mixed monolayer of ω-thiol trimethylammonium chloride and octanethiol (Me$_3$NAu NPs) was purified by repeated suspension, centrifugation, and decantation with dichloromethane.[23] ^{1}H NMR indicated an exchange of original octanethiol for the ω-thiol trimethylammonium chloride ligand by ~70%. The Me$_3$NAu NPs dissolved in pure water without the need for pH adjustment.

Preparation of Floating Bilayers. For the preparation of the floating lipid bilayer samples, highly polished (<3 Å roughness) silicon single 111 crystals of a 8 × 5 cm^2 surface and a 1 cm thickness were used as substrates. Prior to use, the substrates were sonicated in chloroform and acetone and then exposed to a continuous flow of ozone for 30 min in order to render the substrate surface highly hydrophilic.

The first three lipid layers were deposited according to the Langmuir−Blodgett method. A chloroform solution of DSPC was spread onto the water subphase of a computer-controlled NIMA 611 Langmuir−Blodgett trough (surface area of 600 cm^2; Nima Technology Ltd., Coventry, England) equipped with one barrier, an electronic pressure sensor with precut paper Wilhelmy plates (wet perimeter 20.6 mm; weight 80 mg m^{-2}), and a dipper and well (63 × 180 mm^2; 70 mm deep) at one end, until a slight change in surface pressure became measurable (≤0.2 mN m^{-1}). The temperature of the subphase water was held constant using a refrigerating/heating circulator (Fisher Scientific) set to 20 °C. After an equilibration time of ~30 min, the monolayer was compressed at a rate of 20 cm^2 min^{-1} to a surface pressure of 40 ± 0.1 mN m^{-1}. Three vertical depositions onto the silicon substrate, beginning upward, resulted in an adsorbed lipid bilayer with a floating lipid monolayer resting on top.[20] The transfer ratios for these layers were 0.94 ± 0.5. The floating lipid bilayer was completed by a final horizontal Langmuir−Schaefer deposition of the same lipid as the three first layers (DSPC) to obtain symmetric zwitterionic bilayers. During this final step, the substrate with the floating bilayer was directly placed onto a PTFE lid filled with ultrapure water.[20] The sample cell was tightly closed and transferred to an aluminum holder. At the beamline, the holder was connected to a water circulation bath (Haake) with a feedback in temperature from a PT100 resistance sensor placed close to the PTFE lid, in order to control the sample temperature. The samples were annealed for one to two hours around 10 °C above the gel/liquid phase transition temperature (DSPC: T_m = 55 °C).[19] The PTFE lid included inlet and outlet holes that were used to rinse the sample with different subphases: D$_2$O, silicon matched water (SMW), H$_2$O, and aqueous nanoparticle solutions of different concentration.

Neutron Reflectometry. Reflectivity measurements were performed on the D17[29] reflectometer at the ILL, Grenoble (France) in the time-of-flight mode, variable resolution = 1−10%, λ range between 2 and 20 Å, with two incoming angles of 0.7 and 3°. The cell was oriented vertically and kept in position while changing solvents and temperature. Measurements were performed at the silicon−water interface, the beam coming from the silicon block side. In a neutron reflectivity experiment, the ratio between the intensities of the reflected and incoming beams, R, is measured as a function of Q_z, the momentum transfer perpendicular to the interface.[30] Reflectivity is related to the scattering length density (SLD) across the interface by the approximate relation:

$$R(Q_z) \sim \frac{16\pi^2}{Q_z^2} |\hat{\rho}(Q_z)|^2 \tag{1}$$

valid in the Born approximation.[31] $\hat{\rho}(Q_z)$ is the Fourier transform of the SLD profile $\rho(z)$ along the normal to the interface, giving

Table 1. Structural Parameters of the Pristine DSPC Lipid Bilayers System (Sample 1) in D_2O at 25 °C[a]

layer	thickness (Å)	SLD ($\times 10^{-6}$ Å^{-2})	solvent (%)	roughness (Å)	area per mol (Å^2)
Si	∞	2.07	0	4	–
SiO$_2$	8.0 ± 0.2	3.47	19 ± 0.4	4	–
heads	8 ± 0.1	1.82	41 ± 1	5	
tails	19.57 ± 0.03	−0.41	10 ± 1	5	59.8 ± 0.2
tails	19.57 ± 0.03	−0.41	10 ± 1	5	
heads	8 ± 0.1	1.82	41 ± 1	5	
water	13.3 ± 0.2	6.0 ± 0.01	100	5	–
heads	13.6 ± 0.2	1.82	65.4 ± 1	5	
tails	22.0 ± 0.04	−0.41	19.8 ± 1	5	59.9 ± 0.2
tails	22.0 ± 0.04	−0.41	19.8 ± 1	5	
heads	13.6 ± 0.2	1.82	65.4 ± 1	5	

[a]The values without error were fixed or kept at their nominal values.

information about the composition of each layer and about its structure. The SLD is given by

$$\rho(z) = \sum_j b_j n_j \tag{2}$$

where n_j is the number of nuclei per unit volume, and b_j is the scattering length of nucleus j. The method of analysis often used for specular reflection data involves the construction of a model of the interface that may be represented by a series of parallel layers of homogeneous material. Each layer is characterized by an average SLD, weighted on all of its nonwater components, and a thickness. These parameters are used to calculate a model reflectivity profile by means of the optical matrix method.[31] The interfacial roughness between any two consecutive layers may also be included in the model by the Abeles method.[32] The calculated profile is compared to the measured profile, and the quality of fit is assessed by using χ^2 in the least-squares method. The model parameters are then adjusted to minimize χ^2.

If the technique is appropriately used, it can reveal structural details down to the fraction of nanometer scale. The use of a combination of hydrogenated and deuterated material (contrast variation) can substantially change the reflectivity curve of a system while maintaining almost the same chemical structure. Experience on this kind of system and on similar ones suggests that the measurement of reflectivity curves from three or more contrasts, combined with standard physical hypotheses, are necessary and sufficient for extracting a unique model of the interface.

Data were analyzed using Motofit,[33] allowing simultaneous fitting of data sets from the same sample under different contrast conditions. In normal operation, Motofit considers each slab in the system to be independent of the adjacent slabs. However, this can lead to interparameter correlation when describing lipid systems. For example, separate layers are required to model the tail and headgroup region of a single lipid layer. The overall SLD of each layer depends on the packing (hydration) of each molecule. Since a headgroup is connected to two tail groups, the SLDs of each layer are covariant. This problem can be eliminated by reparameterising the model using physically relevant parameters. Each lipid layer was described in terms of a thickness (T_x), volume (V_x), and scattering length (b_x) of the tail ($x =$ t) and head ($x =$ h) sublayers, their roughness, and area per molecule, A. The values of the scattering lengths are determined by the composition of the lipid segment, whereas their volumes, V_h and V_v, are tabulated in literature.[35] The volume fraction of tails in a tail layer is given by V_t/AT_v, the volume fraction of heads in a head layer is given by V_h/AT_h. The rest of the volume in a given layer is occupied by water molecules, $1-(V_x)/(AT_x)$. The overall SLD of a head or tail layer is given by

$$\rho_x = \frac{b_x}{AT_x} + \rho_{solv}\left(1 - \frac{V_x}{AT_x}\right) \tag{3}$$

When describing each lipid layer, the only parameters allowed to vary during the fit are A, T_h, T_v and the roughness of each sublayer. T_h and

T_t are constrained between sensible limits, and the use of the same A for the tail and head groups for a given lipid layer encodes and enforces a one-to-one correspondence between the two. The Differential Evolution fitting algorithm was used to fit the data with the parameter uncertainties being obtained from their covariance matrix. All errors are reported as ±1 standard deviation. The presence of an inplane structure at the interface, arising from density fluctuations in either a regular or irregular pattern, produce an off-specular component to the scattered radiation.[34] Theoretical descriptions of the off-specular scattering, relating to parameters such as size, height, and domain−domain correlations of the surface features are being developed. For thin films, like those described in this work, the neutron off-specular signal is weak and difficult to analyze. In these cases synchrotron radiation is better suited for a quantitative analysis.[36] However, some qualitative information can be obtained by neutron off-specular scattering.

■ EXPERIMENTAL RESULTS

After annealing the pristine floating lipid bilayers above the gel/liquid phase transition temperature, they were characterized at two or three different contrasts: fully deuterated water (D_2O), water (H_2O), and a solution of H_2O and D_2O index matched to the SLD of the silicon block. The SLD of the bulk phases were fitted to account for possible incomplete exchange of solvent in the cell. For this reason, in some cases this fitted value of the SLD of the bulk phase was slightly different from the tabulated one. The complete characterization of the lipid bilayers at the three solvent contrasts were performed after their annealing above the phase transition temperature. The corresponding reflectivity profiles are shown in the Supporting Information. The annealing process was performed to remove possible structural defects in the membrane that may have occurred during the preparation of the double bilayer below the phase transition temperature and demonstrate that the lipid double bilayers remained stable at increased temperature in the fluid phase.

DSPC Floating Bilayer with Cationic Me$_3$Au Nanoparticles. The first annealed DSPC floating bilayer (sample 1) was measured at three contrasts and at a temperature of 25 °C. The reflectivity profiles at different contrasts were fitted according to the model described above with the area per molecule shared between the heads and the tails of each lipid bilayer. We made the further assumption that the bilayers are symmetric in order to reduce the fitting parameters. The reflectivity curves and the corresponding SLD profiles are displayed in the Supporting Information. The structural data obtained from the fits are listed in Table 1 and are in agreement with previous experimental results.[20]

The exposure of the DSPC floating bilayer to an aqueous solution of 0.01 mg mL^{-1} cationic Me$_3$NAu NPs at 25 °C did not significantly alter the reflectivity profile. Preliminary work showed that the floating bilayer completely disintegrated and dissolved when the temperature is taken above the liquid−gel transition to 64 °C in the presence of the cationic Me$_3$NAu NPs (data not shown). Sample 1 was, therefore, only heated to 53 °C (i.e., slightly below the liquid−gel transition
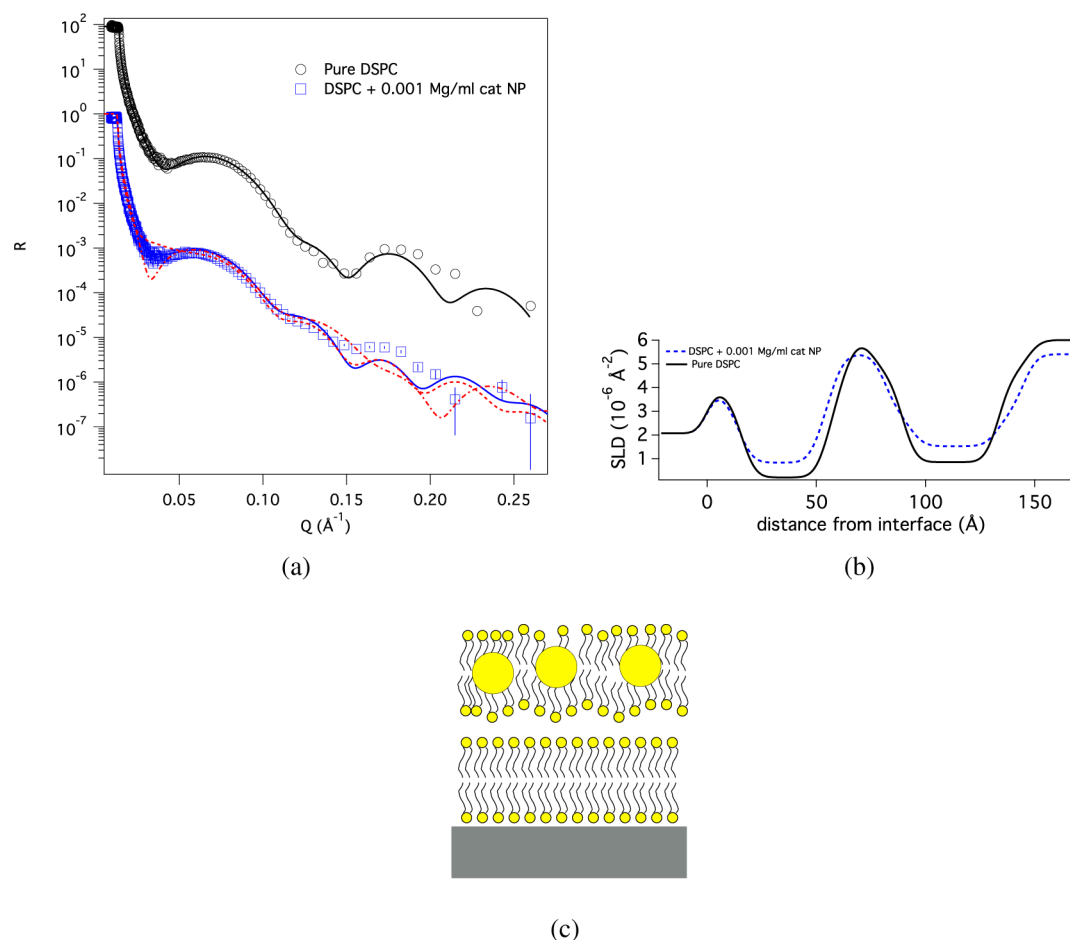
(a)

(b)

(c)

Figure 1. (a) Reflectivity profiles of the DSPC bilayers system (sample 1) measured in the pristine form and in the presence of 0.01 mg mL^{-1} cationic Me$_3$NAu NPs nanoparticles at 25 °C. The reflectivity profile of the pure DSPC double bilayer is offset. Continuous black and blue lines are the best fits to the measured data. The red lines represent the results of the fitting models that include the presence of the cationic Me$_3$NAu NPs also in the supported bilayer (dash) and the absence of NPs in the lipid bilayers (dashed dotted line). (b) SLD profiles of the sample are extracted from the fits to the measurements. (c) The sketch shows structural details deduced from the fitting parameters of the reflectivity curves.

Table 2. Structural Parameters of the DSPC Lipid Bilayers System (Sample 1) in the Presence of 0.01 mg mL^{-1} Cationic Me$_3$NAu NPs at 25 °C^a

layer	thickness (Å)	SLD ($\times 10^{-6}$ Å^{-2})	solvent (%)	roughness (Å)	area per mol Å^2
Si	∞	2.07	0	4	–
SiO$_2$	8.8 ± 0.3	3.47	19 ± 3	4	–
heads	6.3 ± 0.4	1.82	39 ± 4	5	73.5 ± 0.2
tails	18.30 ± 0.03	−0.41	21.5 ± 0.4	5	
tails	18.30 ± 0.03	−0.41	21.5 ± 0.4	5	
heads	6.3 ± 0.4	1.82	39 ± 4	5	
water	23.7 ± 0.5	5.40 ± 0.01	100	5	–
heads	11.8 ± 0.5	1.82	30 ± 4	5	–
tails	20 ± 1	1.47 ± 0.03	2 ± 1	5	–
tails	20 ± 1	1.47 ± 0.03	2 ± 1	5	–
heads	11.8 ± 0.5	1.82	30 ± 4	5	–

^{a}The values without error were fixed or kept at their nominal values.

temperature) and maintained its integrity. The temperature was then gradually brought back to 25 °C. The reflectivity was measured in the presence of the Me$_3$NAu NPs and after exchanging the sample volume with pure water. The rinsing did not cause any alteration in the reflectivity profile, indicating that the structural configuration of the nanoparticle/lipid system was stable at this point.

The model used to fit the data in the presence of NP was slightly different compared to that used for the pure bilayer. The changes of the reflectivity profile could be accounted by increasing the SLD of the

tail region of the floating bilayer. This can be explained by the inclusion of some AuNPs in this region of the bilayer. However, the SLD of the NP is difficult to model, since the conformation of the alkyl chain tethered to the gold core is hard to estimate in the lipid bilayer. Therefore, a simplified model of the lipid/NP system was used. The floating bilayer with embedded NPs was modeled with a slab of higher SLD, whose value was obtained from the fit. The measurements at different contrasts served to differentiate between the effect of the
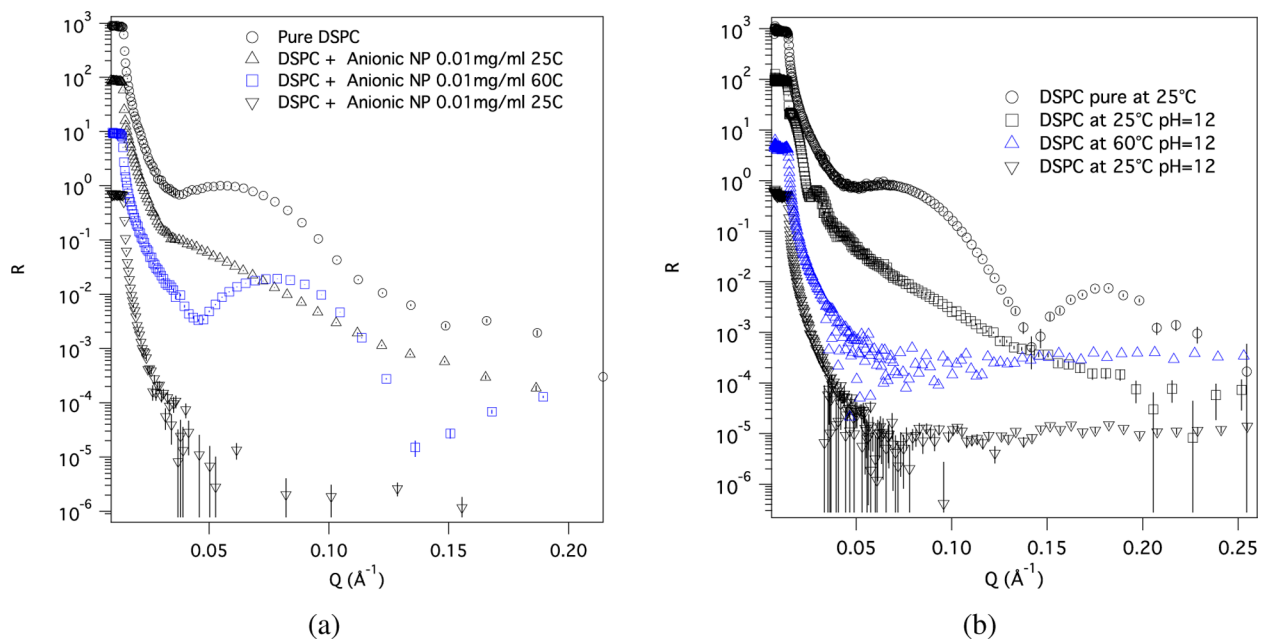
Figure 2. (a) Reflectivity profiles of the pristine DSPC lipid bilayers system (sample 2) measured at different conditions: pure lipid membrane at 25 °C (○) in the presence of 0.01 mg mL^{-1} anionic COOHAu NPs at the 25 °C, pH = 12 (△), and at 25 °C after a stopover at 60 °C, pH = 12 (▽). (b) Reflectivity profiles of the DSPC floating bilayer used as a control at different conditions: pure lipid membrane at 25 °C (○), 25 °C (□), pH = 12, and at 60 °C (△), pH = 12. The data are off-set for better visualization.
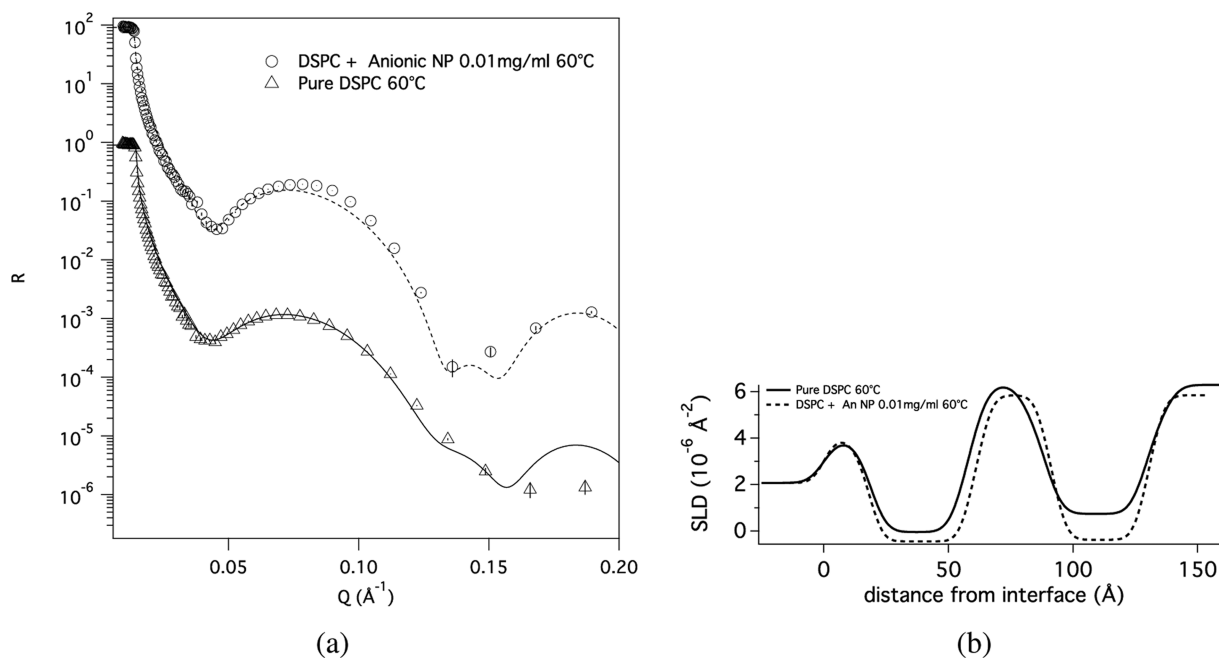

Figure 3. (a) Reflectivity profiles of the pristine DSPC lipid bilayer system (sample 2) measured at different conditions: pure lipid membrane at 60 °C, in the presence of anionic COOHAu NPs at 60 °C. The dashed and solid lines are fits to the measured data with and without 0.01 mg mL^{-1} nanoparticles, respectively. (b) SLD profiles extracted from the fits to the reflectivity profiles of the DSPC floating bilayer before and after exposure to the anionic COOHAu NPs at 60 °C. The reflectivity profiles are off-set for better visibility.

solvent molecules entering the lipid bilayer and the inclusion of AuNPs.

Figure 1 displays the scattering curves obtained from sample 1 in its pristine form, after the addition of cationic Me$_3$NAu NPs at 25 °C, after the temperature changes, and after rinsing the sample with pure water. Only the measurement at one contrast (D$_2$O) is visualized, those performed at the other contrast can be found in the Supporting Information. The structural details listed in Tables 1 and 2 point out that the main effect is an increase of the SLD in the tail region of the

floating lipid bilayer, which is consistent with the inclusion of the nanoparticle gold core (SLD = 4.5 × 10^{-6} Å^{-2}) in this part of the bilayer, accompanied by a displacement of water molecules. The presence of the cationic Me$_3$NAu NPs reduced the individual thickness of supported and floating bilayer, but the total thickness of the lipid systems remained constant due to the increase of the interstitial water layer.

Alternative ways to analyze the changes in the reflectivity profiles of the lipid system in the presence of cationic Me$_3$NAu NPs were also

Table 3. Structural Parameters of the Pure DSPC Lipid Bilayers System (Sample 2) at 60 °C[a]

layer	thickness (Å)	SLD (×10⁻⁶ Å⁻²)	solvent (%)	roughness (Å)	area per mol Å²
Si	∞	2.07	0	4	–
SiO₂	13	3.47	6 ± 4	4	–
heads	6.3 ± 1	1.82	36 ± 10	5	70.0 ± 0.3
tails	18.0 ± 0.1	−0.36	5 ± 1	5	
tails	18.0 ± 0.1	−0.36	5 ± 1	5	
heads	6.3 ± 1	1.82	36 ± 10	5	
water	20 ± 1	6.29 ± 0.01	100	5	–
heads	8.6 ± 0.1	1.82	56 ± 1	5	74.8 ± 0.3
tails	19.2 ± 0.1	−0.36	17 ± 1	5	
tails	19.2 ± 0.1	−0.36	17 ± 1	5	
heads	8.6 ± 0.1	1.82	56 ± 1	5	

[a]The values without error were fixed or kept at their nominal values.

considered: the data was fit under the hypothesis that (i) the NP did not enter the lipid (red dashed−dotted line in Figure 1) and (ii) they were embedded in both supported and floating lipid bilayers (red dashed line in Figure 1). In both cases, the model failed to reach an acceptable fit with the data, especially at lower Q.

The molecular area of the supported bilayer in the presence of NPs is around 20% larger than the corresponding number of the lipid system without NPs, yet no fitting model, including the presence of Me₃NAu NPs, in this layer is consistent with the experimental results. A possible reason for this increased value could be the loss of material during solvent exchange and fluctuation of the bilayers occurring at 53 °C, few degrees below the liquid−gel transition. In pure systems, fluctuations and rinsing do not lead to the loss of material on the adsorbed layer but only on the floating bilayer.[36] Nevertheless, the presence of Me₃NAu NPs may have had a destabilizing effect on both bilayers.

DSPC Floating Bilayer with Anionic COOHAu Nanoparticles. The reflectivity profiles of the second annealed DSPC sample (sample 2) were measured at 25 °C at three different contrasts and are displayed along with the SLD profiles and a table containing the structural details extracted from the fits in the Supporting Information.

The exposure of the DSPC floating bilayer to a 0.01 mg mL⁻¹ anionic COOHAu NPs aqueous solution (pH 12) at 25 °C led to drastic effects in the reflectivity profile that are difficult to evaluate. Initially, the two minima in the reflectivity profile that are characteristic of a floating lipid bilayer disappeared upon first contact with the COOHAu NPs at 25 °C, as seen in Figure 2 (△). However, once the temperature was above the gel−fluid phase transition at 60 °C, the minima reappeared and became even more pronounced. Back at 25 °C, the intensity of the reflectivity decreased remarkably (see ▽ in 2). This change was accompanied by a rise in the off-specular scattering, which was likely a result of an increase in roughness of the measured surface, possibly due to a damage of the lipid layer and/or adsorption of COOHAu NPs.

To prove that the reappearance of the two minima was caused by the presence of the anionic COOHAu NP and not by the variation in pH, a control experiment with the same temperature cycle was performed in the presence of an aqueous solution of pH 12 without the COOHAu NPs. The resulting reflectivity profiles are shown in Figure 2b. After the injection of the pH 12 solution at 25 °C, a series of oscillations appeared, which were probably due to an ~500 Å thick layered structure. This structure was not stable since the reflectivity profile evolved with time (not shown). Once the sample temperature was raised to 60 °C, the measured data did not differ from a Fresnel reflectivity profile, indicating that the lipid model membrane had completely broken apart and dissolved. Even lowering the temperature back to 25 °C did not lead to any further changes, and the lipid bilayer remained disintegrated. We can assume, therefore, that the anionic COOHAu NPs reduced the damage to the fluid phase lipid bilayer that would have occurred in the presence of extreme alkaline pH.

Figure 3a shows the reflectivity profiles of the pristine floating bilayer and the floating bilayer in the presence of the anionic

COOHAu NPs at 60 °C. Both reflectivity profiles were fit to the model with shared area per molecule for the heads and tails and did not require any COOHAu NP inclusion into the lipid membrane to obtain a good fit (see Figure 3a). The resulting SLD profiles are shown in Figure 3b, and the structural details are listed in Tables 3 and 4. The

Table 4. Structural Parameters of the DSPC Lipid Bilayers System (Sample 2) in the Presence of 0.01 mg mL⁻¹ Anionic COOHAu NPs at 60 °C[a]

layer	thickness (Å)	SLD (×10⁻⁶ Å⁻²)	solvent (%)	roughness (Å)	area per mol Å²
Si	∞	2.07	0	4	–
SiO₂	13 ± 5	3.47	6.3 ± 5	4	–
heads	6 ± 1	1.82	19 ± 6	4	61 ± 0.5
tails	18 ± 1	−0.36	0 ± 6	4	
tails	18 ± 1	−0.36	0 ± 6	4	
heads	6 ± 5	1.82	19 ± 6	4	
water	25 ± 6	5.84 ± 0.1	100	4	–
heads	5 ± 4	1.82	23.7 ± 6	4	70 ± 1
tails	17 ± 1	−0.36	0 ± 6	4	
tails	17 ± 1	−0.36	0 ± 6	4	
heads	5 ± 4	1.82	23.8 ± 6	4	

[a]The values without error were fixed or kept at their nominal values.

principal effect that the COOHAu NPs seem to exert on the lipid bilayers is the dehydration and the thinning of both floating and supported bilayers. The reduction of the roughness of the lipid bilayer by 1 Å improved the quality of the fit.

DISCUSSION

In the previous sections, we have shown the structural changes observed in floating symmetric, neutral DSPC bilayers in the presence of cationic and anionic gold nanoparticles by means of neutron reflectometry experiments.

As noted earlier, the DSPC floating lipid bilayers did not undergo any structural changes upon exposure to the cationic Me₃NAu NPs at 25 °C. However, as soon as the samples were heated close to the phase transition temperature, the fitting model for the measured reflectivity profiles required an SLD increase in the hydrophobic moiety (tail region) of the floating bilayers. Such an increase can be explained by an inclusion of AuNPs ($\rho \sim 4.5 \times 10^{-6}$ Å⁻²) in this part of the lipid system. Once the AuNPs entered the tail region of the floating lipid bilayer, the system was composed of three components (i.e., lipid tails, Me₃NAu NPs, and water molecules). Since we performed the measurements at two different contrasts (D₂O and silicon matched D₂O/H₂O mixture), we can distinguish

between the first two components and the latter. In accordance with the model parameters, the Me₃NAu NPs penetrated into the tail region of the floating lipid bilayer causing a rise in the SLD value and a displacement of the water molecules from this inner region. The thickness of the inner region was 40 Å, which could comfortably accommodate a AuNP of a 20 Å diameter along with tethered ligands (C11-alkyl spacer with a trimethyl ammonium headgroup). The amount of AuNPs that entered the lipid bilayer can be quantified in terms of volume fraction directly from the SLD value of the tail region taken from Table 2. Since the SLD of the hydrocarbon chains and of the molecules tethered to the AuNP are similar, the following equation holds:

$$\rho = \phi_{NP}\rho_{NP} + \phi_{HC}\rho_{HC} \qquad (4)$$

with ρ the SLD, ϕ_{NP} and ϕ_{HC} the volume fractions of the AuNPs and the hydrocarbon chains, respectively, and ρ_{NP} and ρ_{HC} the SLD of the nanoparticles and the hydrocarbon chains, respectively. This contribution does not include the water molecules that are considered in the fitting model in terms of hydration percentage. Hence, the volume fraction of the Me₃NAu NPs in the floating bilayer was $\phi_{NP} = 0.37 \pm 0.02$. The presence of the AuNP inside the lipid bilayer probably augmented the lateral pressure among the lipid molecules also causing a consistent dehydration of the lipid head groups, as can be seen in Table 2. The displacement of water molecules may also be due to the presence of some ligands tethered to the NPs.

If the floating bilayer was heated slightly below the transition temperature to 53 °C, it maintained its structural integrity, enclosing the Me₃NAu NPs in its hydrophobic moiety. If it was heated above the transition temperature to 60 °C, the floating bilayer broke down and dissolved. As permeability in lipid bilayers reaches gradually a maximum in the fluid phase beyond the phase transition temperature,[40] the Me₃NAu NPs become more and more easily embedded into the lipid membrane that might lead to a gradual destabilization of its structure, depending on the quantity of inserted AuNP and may explain the observed difference in lipid membrane behavior.[41]

The symmetric zwitterionic DSPC floating bilayer of sample 2 was exposed to 0.01 mg mL⁻¹ anionic COOHAu NPs at 25 °C, which immediately induced drastic changes in the reflectivity profile. The fingerprint region of the floating bilayer (the minimum at 0.04 Å⁻¹) vanished to reappear again once the sample was heated to 60 °C (i.e., above the gel–fluid transition temperature). The structural details in Table 4 reveal that the nanoparticles strongly dehydrated the heads and tails of the supported and floating lipid bilayer. Since water plays a structure-forming role in lipid bilayers and is essential for the molecular mobility, the hydration degree influences the morphology of the system and can also change the temperature of the gel–liquid phase transition.[44,43] With increasing dehydration, the bilayer thickness should normally increase, while the area per lipid molecule decreases. This affects the bilayer fluidity as well as its lateral and transverse diffusion properties.[45,46] The decrease in the hydration level of the lipid bilayers upon interaction with anionic COOHAu NPs was, however, associated with a decrease in the floating bilayer thickness, indicating its susceptibility to disintegrate and to form lipid vesicles.[47] At this point, the anionic COOHAu NPs may have had a shielding effect on the weakened fluid phase lipid membrane in alkaline pH and may overall have a critical

impact on the integrity and the physiological performance of the biological membranes.

Back at 25 °C, the reflectivity signal decreased substantially again, while the off-specular scattering visibly increased (see the Supporting Information). Whereas the specular reflection provides information about the depth profile of the SLD averaged over the whole sample interface, the accompanying off-specular scattering contains details about the lateral structure of the interface, such as the roughness and structure factor.[48] Evidently, the reduced reflectivity and increased off-specular signal indicate a substantial rise in surface roughness. The origin of this effect is likely found in the interaction of the zwitterionic DSPC bilayers with the anionic charge of the nanoparticles. In accordance with our observations by neutron reflectivity, we can assume that the multivalent anionic COOHAu NPs dynamically interact with the DSPC bilayer surface because no NP adsorption and no incorporation was detected. This interaction possibly induces dehydration with an associated change in the phase transition at an increased temperature of 60 °C.[49,50] In the case of substrate exposure due to lipid bilayer damage, an etching of the SiO₂ surface at alkaline pH can also contribute to an increase of the surface roughness.

Since the COOHAu NPs could only be dissolved at alkaline pH, we repeated the experiment in the presence of an aqueous solution of pH 12 without COOHAu NPs and repeated the same temperature cycle in order to differentiate the effect of pH and that of NPs. The variation of pH induced the formation of an unstable large scale structure at 25 °C, presumably lipid vesicles, and once the temperature reached 60 °C, the lipid bilayer entirely dissolved. Interestingly, this evidence implies that the anionic NP exerts a shielding effect on the lipid bilayer against pH and temperature. This assumption is further supported by preliminary neutron reflectometry studies (not discussed), in which a lower COOHAu NP concentration (0.001 mg mL⁻¹) led to an increased membrane destabilization.

So far, most of the studies on the structural effects of ions on lipid bilayers have been concentrated on mono− and bivalent cations, whereas anions have been examined in a rather limited and nonsystematic way.[42] The elucidation of the precise dehydrating and shielding mechanism lying behind the multivalent anionic COOHAu NP action on the model lipid membrane is beyond the scope of this article, and further, more thorough experiments would be necessary to clarify these phenomena and to describe them in a more detailed and insightful manner.

In agreement with previous experimental and theoretical results, the presented observations show that the charge of the AuNPs has a significant effect on the kind of interaction they have with lipid membranes.[37−39]

Conclusions. Many recent studies have addressed the interaction between nanoparticles and membranes. Besides size, shape,[37,38] ligand structure, and composition, the way in which biological cells take up nanoparticles is significantly affected by the nanoparticles' surface charge. While cationic nanoparticles are thought to enter the cell by membrane diffusion, anionic nanoparticles probably insert through endocytosis. In agreement with these previous experimental and theoretical results, the presented neutron reflectometry experiments have shown that the charge of the AuNPs indeed affects the way nanoparticles interact with lipid bilayers.[37−39] Cationic Me₃NAu NPs tend to pass through the fluid phase of the lipid membrane and remain embedded in the hydrophobic

moiety of the floating bilayer. In contrast, anionic COOHAu NPs do not have the tendency to penetrate the lipid membrane. Rather, they interact with its surface, on the one hand dehydrating it and on the other hand shielding the floating bilayer from extreme alkaline pH in the fluid phase.

Overall, this study shows that the nature of AuNP−lipid membrane interaction depends on the NP surface charge. Further studies that focus on the AuNP concentration and size, as well as lipid bilayer surface charge and composition, are definitely necessary to elucidate further parameters influencing the nanoparticle−cell membrane interaction and their consequences on the membrane structure and integrity. This knowledge is crucial to effectively design safe nanoparticles for biomedical applications and also to define practices and procedures for the secure handling of nanoparticles in general.

■ ASSOCIATED CONTENT

Ⓢ Supporting Information

Fitting plots, tables of fit parameters of the data not shown in the main text, and off-specular scattering are available in the supporting materials. This material is available free of charge via the Internet at http://pubs.acs.org.

■ AUTHOR INFORMATION

Corresponding Author
*M.M.: e-mail, maccarini@ill.fr. S.T.: e-mail, Sabina.Tatur@ alumni.uni-heidelberg.de.

Present Address
∥CEA Grenoble, 38045 Grenoble Cedex 9, France.

Author Contributions
‡S.T. and M.M. contributed equally to this work.

Notes
The authors declare no competing financial interest.

■ ACKNOWLEDGMENTS

■ LIST OF ABBREVIATIONS

AuNP: gold nanoparticle
COOHAu NP: anionic (mercaptoundecanoic acid)-functionalized gold nanoparticle
DSPC: 1,2-distearoyl-sn-glycero-3-phosphocholine
Me₃NAu NP: cationic [N,N,N-trimethyl (11-mercaptoundecyl) ammonium] functionalized gold nanoparticle
SLD: scattering length density
SMW: silicon matched water

■ REFERENCES

(1) Yeh, Y.-C.; Creran, B.; Rotello, V. M. Gold nanoparticles: Preparation, properties, and applications in bionanotechnology. *Nanoscale* **2012**, *4*, 1871−1880.
(2) Dykman, L.; Khlebtsov, N. Gold nanoparticles in biomedical applications: Recent advances and perspectives. *Chem. Soc. Rev.* **2012**, *41*, 2256−2282.
(3) Rana, S.; Bajaj, A.; Mout, R.; Rotello, V. M. Monolayer coated gold nanoparticles for delivery applications. *Adv. Drug Delivery Rev.* **2012**, *64*, 200−216.
(4) Papasani, M. R.; Wang, G.; Hill, R. A. Gold nanoparticles: The importance of physiological principles to devise strategies for targeted drug delivery. *Nanomedicine: Nanotechnol., Biol. Med.* **2012**, *8*, 804− 814.
(5) Zhang, L.; Gu, F. X.; Chan, J. M.; Wang, A. Z.; Langer, R. S.; Farokhzad, O. C. Nanoparticles in medicine: Therapeutic applications and developments. *Clin. Pharmacol. Ther. (N.Y., NY, U.S.)* **2008**, *83*, 761−769.
(6) Giljohann, D. A.; Seferos, D. S.; Daniel, W. L.; Massich, M. D.; Patel, P. C.; Mirkin, C. A. Gold nanoparticles for biology and medicine. *Angew. Chem., Int. Ed.* **2010**, *19*, 3280−3294.
(7) Tiwari, P. M.; Vig, K.; Dennis, V. A.; Singh, S. R. Functionalized gold nanoparticles and their biomedical applications. *Nanomaterials* **2011**, *1*, 31−63.
(8) Sperling, R. A.; Gil, P. R.; Zhang, F.; Zanella, M.; Parak, W. J. Biological applications of gold nanoparticles. *Chem. Soc. Rev.* **2008**, *37*, 1896−1908.
(9) Murphy, C. J.; Gole, A. M.; Stone, J. W.; Sisco, P. N.; Alkilany, A. M.; Goldsmith, E. C.; Baxter, S. C. Gold nanoparticles in biology: Beyond toxicity to cellular imaging. *Acc. Chem. Res.* **2008**, *41*, 1721− 1730.
(10) Lewinski, N.; Colvin, V.; Drezek, R. Cytotoxicity of nanoparticles. *Small* **2008**, *4*, 26−49.
(11) Alkilany, A. M.; Nagaria, P. K.; Hexel, C. R.; Shaw, T. J.; Murphy, C. J.; Wyatt, M. D. Cellular uptake and cytotoxicity of gold nanorods: molecular origin of cytotoxicity and surface effects. *Small* **2009**, *5*, 701−708.
(12) Khlebtsov, N.; Dykman, L. Biodistribution and toxicity of engineered gold nanoparticles: A review of *in vitro* and *in vivo* studies. *Chem. Soc. Rev.* **2011**, *40*, 1647−1671.
(13) Goodman, C. M.; McCusker, C. D.; Yilmaz, T.; Rotello, V. M. Toxicity of Gold nanoparticles functionalized with cationic and anionic side chains. *Bioconjugate Chem.* **2004**, *15*, 897−900.
(14) Mecke, A.; Lee, D.-K.; Ramamoorthy, A.; Orr, B. G.; Banaszak Holl, M. M. Synthetic and natural polycationic polymer nanoparticles interact selectively with fluid−phase domains of DMPC lipid bilayers. *Langmuir* **2005**, *21*, 8588−8590.
(15) Banaszak Holl, M. M. Nanotoxicology: A personal perspective. *Nanomed. Nanobiotechnol.* **2009**, *1*, 353−359.
(16) Ruenraroengsak, P.; Novak, P.; Berhanu, D.; Thorley, A. J.; Valsami-Jones, E.; Gorelik, J.; Korchev, Y. E.; Tetley, T. D. Respiratory epithelial cytotoxicity and membrane damage (holes) caused by amine-modified nanoparticles. *Nanotoxicology* **2012**, *6*, 94−108.
(17) Hirano, A.; Yoshikawa, H.; Matsushita, S.; Yamada, Y.; Shiraki, K. Adsorption and disruption of lipid bilayers by nanoscale protein aggregates. *Langmuir* **2012**, *28*, 3887−3895.
(18) Boon, J. M.; Smith, B. D. Chemical control of phospholipid distribution across bilayer membranes. *Med. Res. Rev.* **2002**, *22*, 251− 281.
(19) Avanti Lipids. Phase Transition Temperatures for Glycerophospholipids. http://avantilipids.com/ (accessed Oct 2, 2012).
(20) Charitat, T.; Bellet-Amalric, E.; Fragneto, G.; Graner, F. Adsorbed and free lipid bilayers at the solid−liquid interface. *Eur. Phys. J. B* **1999**, *8*, 583−593.
(21) Fragneto, G.; Charitat, T.; Daillant, J. Floating lipid bilayers: Models for physics and biology. *Eur. Biophys. J.* **2012**, *41*, 863−874.
(22) Fragneto, G.; Charitat, T.; Bellet-Amalric, E.; Cubitt, R.; Graner, F. Swelling of Phospholipid Floating Bilayers: The Effect of Chain Length. *Langmuir* **2003**, *19*, 7695−7702.
(23) McIntosh, C. M.; Esposito, E. A.; Boal, A. K.; Simard, J. M.; Martin, C. T.; Rotello, V. M. Inhibition of DNA transcription using cationic mixed monolayer protected gold clusters. *J. Am. Chem. Soc.* **2001**, *123*, 7626−7629.
(24) Brust, M.; Walker, M.; Bethell, D.; Schiffrin, D. J.; Whyman, R. Synthesis of Thiol-derivatised Gold Nanoparticles in a Two-phase Liquid−Liquid System. *J. Chem. Soc., Chem. Commun.* **1994**, 801−802.
(25) Tatur, S.; Badia, A. Influence of hydrophobic alkylated gold nanoparticles on the phase behavior of monolayers of dppc and clinical lung surfactant. *Langmuir* **2012**, *28*, 628−639.
(26) Hostetler, M. J; Green, S. J; Stokes, J. J; Murray, R. W. Monolayers in three dimensions: Synthesis and electrochemistry of ω-

functionalized alkanethiolate-stabilized gold cluster compounds. *J. Am. Chem. Soc.* **1996**, *118*, 4212−4213.

(27) Simard, J. M.; Briggs, C.; Boal, A. K.; Rotello, V. M. Formation and pH-controlled assembly of amphiphilic gold nanoparticles. *Chem. Commun. (London)* **2000**, *19*, 1943−1944.

(28) Tien, J.; Terfort, A.; Whitesides, G. M. Microfabrication through electrostatic self-assembly. *Langmuir* **1997**, *13*, 5349−5355.

(29) Cubitt, R.; Fragneto, G. D17: The new reflectometer at the ILL. *Appl. Phys. A: Mater. Sci. Process.* **2002**, *74*, S329−S331.

(30) Penfold, J.; Thomas, R. K. The application of the specular reflection of neutrons to the study of surfaces and interfaces. *J. Phys.: Condens. Matter* **1990**, *2*, 1369−1412.

(31) Born, M.; Wolf, E. *Principles of Optics*. London: Pergamon Press Ltd, 1959.

(32) Abeles, F. La théorie générale des couches minces. *J. Phys. Radium* **1950**, *11*, 307−310.

(33) Nelson, A. Co-refinement of multiple contrast neutron/X-ray reflectivity data using MOTOFIT. *J. Appl. Crystallogr.* **2006**, *39*, 273−276.

(34) Pynn, R. Neutron scattering by rough surfaces at grazing incidence. *Phys. Rev. B* **1992**, *45*, 602−612.

(35) Arment, R. S.; Uitto, O. D.; Feller, S. E. Phospholipid component volumes: Determination and application to bilayer structure calculations. *Biophys. J.* **1998**, *75*, 734−744.

(36) Daillant, J.; Bellet-Amalric, E.; Braslau, A.; Charitat, T.; Fragneto, G.; Graner, F.; Mora, S.; Rieutord, F.; Stidder, B. Structure and fluctuations of a single floating lipid bilayer. *Proc. Natl. Acad. Sci. U.S.A.* **2005**, *102*, 11639−11644.

(37) Chithrani, B. D.; Ghazani, A. A.; Chan, W. C. W. Determining the size and shape of gold nanparticle uptake into mammalian cells. *Nano Lett.* **2006**, *6*, 662−668.

(38) Chithrani, B. D.; Chan, W. C. W. Elucidating the Mechanism of Cellular Uptake and Removal of Protein−Coated Gold Nanoparticles of Differenct Sizes and Shapes. *Nano Lett.* **2007**, *7*, 1542−1550.

(39) Lin, J.; Zhang, H.; Chen, Z.; Zheng, Y. Penetration of lipid membranes by gold nanoparticles: Insights into cellular uptake, cytotoxicity, and their relationship. *ACS Nano* **2010**, *4*, 5421−5429.

(40) Xiang, T.-X.; Anderson, B. D. Dipalmatoylphosphatidylcholine bilayer membranes for permeant size and shape. *Biophys. J.* **1998**, *75*, 2658−2671.

(41) Blicher, A.; Wodzinska, K.; Fidorra, M.; Winterhalter, M.; Heimburg, T. The temperature dependence of lipid membrane permeability, its quantized nature, and the influence of anesthetics. *Biophys. J.* **2009**, *96*, 4581−4591.

(42) Aroti, A.; Leontidis, E.; Dubois, M.; Zemb, T. Effects of monovalent anions of the hofmeister series on DPPC lipid bilayers Part I: Swelling and in-plane equations of state. *Biophys. J.* **2007**, *93*, 1580−1590.

(43) Przyczyna, A.; Różycka-Roszk, B.; Langner, M. The Effect of selected anions on dipalmitoylphosphatidylcholine phase transitions. *Z. Naturforsch.* **2002**, *57c*, 712−716.

(44) Khakimov, A. M.; Rudakova, M. A.; Filippov, A. V. Water state and diffusion through lipid bilayers: Effect of hydration degree. *Cell Biophys.* **2007**, *52*, 840−849.

(45) Hristova, K.; White, S. H. Determination of the hydrocarbon core structure of fluid dioleoylphosphocholine (DOPC) bilayers by X-ray diffraction using specific bromination of the double-bonds: Effect of hydration. *Biophys. J.* **1998**, *74*, 2419−2433.

(46) Pace, R. J; Chan, S. I. Molecular motions in lipid bilayers. III. Lateral and transverse diffusion in bilayers. *J. Chem. Phys.* **1982**, *76*, 4241−4247.

(47) Bangham, A. D.; Horne, R. W. Negative staining of phospholipids and their structural modification by surface-active agents as observed in the electron microscope. *J. Mol. Biol.* **1964**, *8* (5), 660−668.

(48) Lauter-Pasyuk, V. Neutron grazing incidence techniques for nano-science. *Collect. Soc. Fr. Neutron.* **2007**, *7*, s221−s240.

(49) Bryant, G.; Koster, K. Dehydration of solute−lipid systems: Hydration forces analysis. *Colloids Surf., B* **2004**, *35*, 73−79.

(50) Petrache, H. I.; Zemb, T.; Belloni, L.; Parsegian, A. Salt screening and specific ion adsorption determine neutral−lipid membrane interactions. *Proc. Natl. Acad. Sci. U.S.A.* **2006**, *103* (21), 7982−7987.